An Investigation of Swirling Flow in a Cylindrical Tube

Tae-Hyun Chang*

Division of Mechanical and Automation engineering, Kyungnam University, 449 Wolyoung Dong, Masan, Kyungnam, Korea

Hee-Young Kim

Graduate Student. Division of Mechanical and Automation engineering, Kyungnam University, 449 Wolyoung Dong, Masan, Kyungnam, Korea

An experimental study was performed for measuring velocity and turbulence intensity in a circular tube for Re=10,000, 15,000 and 20,000, with swirl and without swirling flow. The velocity fields were measured using PIV techniques and swirl motion was produced by a tangential inlet condition. Some preliminary measurements indicated that over the first 4 diameter, two regions of flow reversal were set up (the so called 2-cell structure). At the highest Reynolds numbers, the maximum values of the measured axial velocity components had moved toward the test tube wall and produce more flow reversal at the conter of the tube. As the Reynolds number increased, the turbulence intensity of swirling flow at the tube inlet also increased.

Key Words : Tangential Inlet Condition, Intensity of Swirl, 2-Cell Structure, Flow Reversal

Nomenclature

C_{fg} : Cross-correlation coefficients
D : Diameter of the test tube
f_i : Gray levels of the pixels within the correlation region
g_i : Gray levels of the pixels within the correlation region
L : Axial distance between the exit of the swirl chamber and the inlet of test tube
n : The pixel number of the correlation area
r : Radial position
R : Radius of the test tube
u : Fluctuating velocity
U : Time averaged axial velocity
$\bar{U}$: Mean average axial velocity
X : Axial coordinate
y : Distance from the wall

* Corresponding Author,
E-mail : changtae@hanma.kyungnam.ac.kr
TEL : +82-55-249-2613; **FAX** : +82-55-249-2617
Division of Mechanical and Automation Engineering, Kyungnam University, 449 Wolyoung Dong, Masan, Kyungnam, Korea. (Manuscript **Received** September 7, 2001; **Revised** October 22, 2001)

1. Introduction

During the past three decade or so, the characteristics of turbulent swirling flow have been studied extensively because of its great technological and scientific importance. It is well known that swirling the flow improves heat transfer in duct flow. The reason for this is due to the effect of streamline curvature associated with the tangential velocity component.

Many experimental investigations have been carried out in turbulent swirling flow with and without heat transfer. A large proportion of them deal specifically with the types of swirl conditions that exist in combustion situations, and these are summarized in the excellent review paper of Lilley(1973). One of the earliest important studies of turbulent swirl flow was carried out by Nuttall in 1953. He was one of the first to observe the flow characteristics of swirling flow in circular tubes by using flow visualization techniques (dye injection method).

All subsequent experimental observation have

been directed at investigating this flow structure using different observation techniques. In this respect, the early investigations such as those of Binnie et al. (1955) and Chigier et al. (1967), used pitot tubes. Others such as Nuttall(1953), Binnie(1957) and Sparrow et al. (1984) used flow visualization techniques similar to Nuttall's experiments to confirm the existence of flow reversal regimes. Later, investigations by Rose (1962), Roberts et al. (1971), Wolf et al. (1963) and Weske et al. (1984) used more sophisticated measurement techniques such as hot wire anemometry.

Since the swirl flows have strong three-dimensionality, it is not so easy to get correlative data bundles from the measurement results obtained by pointwise measurement techniques. This means that the data obtained by the conventional measurement techniques such as LDV (Laser Doppler Velocimetry), hot wire, and pitot tube can not be used for unsteady analysis of the swirl flow. Field measurement is one of the most appropriate techniques for the unsteady analysis on swirl flows. Unfortunately, most of the previous studies have been issuing not with quantitative but with qualitative experimental results.

The main objective of this study is to construct a database on swirl flows using PIV technique (Thinker's EYES) , which will play an important role in designing thermal fluid machineries in which swirling is playing as a main source of heat and mass transport.

2. General Layout of the Isothermal Apparatus

A schematic layout of the general apparatus is given in Fig. 1. Water was drawn through a swirl generating chamber, the test tube working section, flow metering and main plenum chamber by a centrifugal pump. Adjustment of the rpm controller on the pump discharge side provided a coarse variation of water flow rate, with finer control being achieved with a valve located in the side of the plenum chamber. The isothermal test section was of 50.8mm inside diameter with a wall thickness of 6.36mm and length of 3m, and was

Fig. 1 Experimental apparatus for swirling flow and experimental conditions

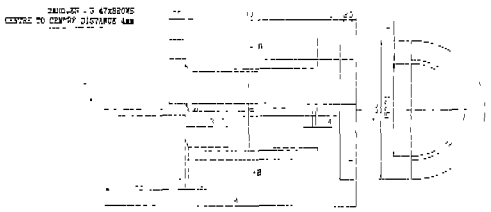

Fig. 2 Swirl generator arrangement (All dimensions are in mm)

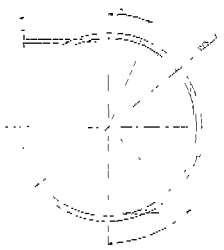

Fig. 3 B-B section views through swirl generator

manufactured from Perspex. Figures 2 and 3 are showing the swirl generator. The swirl generator consisted of two perspex cylinders of the following dimensions: an outer chamber of outside diameter 241mm, length 1069mm and wall thickness 6.35mm: the swirl generator itself of outside diameter 165.6mm, length 250mm and wall thickness 6.35mm.

The PIV technique was used for the bulk of the isothermal flow velocity measurements. Thinker's EYES was used for image grabbing and image selecting to be processed that are necessary for PIV measurement. The used algorithm is the gray-level cross-correlation method(Kimura et al. 1986). An Ar-ion laser (500mW) was used for visualization and a CCD camera was installed perpendicularly to the visualized section of the flow. AOM(Acoustic Optical Modulator) was used to control the time of lighting the laser

source and to shorten the time interval of the field images of one frame. Further, in order to increase the traceability of correct vectors even in strong three-dimensional flow, this AOM was used in this study. Once the vectors were obtained by the PIV system having the AOM system, the obtained vectors represent two components (u, v) of velocity vectors in the two-dimensional plane. The grabbed frame image is separated into two fields, odd and even fields. Vacant odd field data in the even field image were obtained by interpolating the data of the upper and the lower even fields. And the vacant even fields in the odd field image are interpolated by averaging the upper and the lower odd field data to get the complete field images. For these field images, the velocity vectors were obtained by using the PIV algorithm. The calculating time on the host computer (Pentium 550MHz) was about 3 minutes in the case of the grid 35×70, the radius for the searching area was set to 25 pixels, the size for the correlation area was set to 32×32 pixels. To eliminate erroneous vectors, an error vector elimination method (Hojo et al. 1995) based on the continuous flow condition was adopted.

In order to prohibit the refractive effects of the circular pipe on the results, a square box was installed, which recovered the refracted light waves from the visualized section of the flow.

3. PIV System

The light from an Ar-ion laser (500mW) passes through a probe to make two-dimensional light sheet. In order to make coded images of the tracer particles on one frame, the AOM (Acoustic-Optical Modulator) is used. The AOM controller is synchronized with the camera and sends a carrier signal to the AOM unit with 100 MHz , which enables the AOM system to work as an electric shutter (Kobayashi et. al, 1991).

The images taken through the camera are captured with a frame grabber (DT3155) and converted into 8 bits levels (256) on the host computer.

In order to get velocity vectors, a process for particle identification is done for the extraction of velocity vectors. This is based upon the two-fields cross-correlation method in which the coordinate indicating the maximum coefficient is assumed to be a vector terminal point (Kimura et al., 1986, Utami and Blackwelder, 1991). Equation (1) is a formula to calculate the cross-correlation coefficients.

$$C_{fg}=\frac{\sum_{i=1}^{n^2}(f_i-\bar{f_i})(g_i-\bar{g_i})}{\sqrt{\sum_{i=1}^{n^2}(f_i-\bar{f_i})^2\sum_{i=1}^{n^2}(g_i-\bar{g_i})^2}} \quad (1)$$

Here, f_i, and g_i mean gray levels of the pixels within the correlation region and, '-' over these letters indicates the average value of the gray levels of the pixels within the correlation region. n^2 means the pixel number of the correlation area. The terminal point of the velocity vector is decided when the calculated coefficient is the maximum value in the searching area.

The grabbed frame image is separated into two fields, odd and even fields. The velocity vectors are obtained on the two field images.

The digitized images are stored with 256 gray levels in integer values and these values are transformed into ASCII files for image processing. Positional data on each pixel on the 2-dimensional image are produced and its gray level distribution is obtained from the image files. In order to eliminate the noise disturbance that greatly affect the reliability of the resulted velocity vectors, the background image was subtracted from each image before processing. In this study, the background image is obtained by averaging about 200 consecutive field images.

The calculating time on the host computer was about 2 minutes in the case that the grid for velocity vector extraction was set to 40×120, the radius for the searching area was set to 30 pixels, the size for the correlation area was set to 30×30 pixels. Since there is a positional uncertainty with maximum ±1 pixel when the terminal point of the velocity vector is obtained by the PIV based on pixel resolution, the sub-pixel interpolation method (Utami and Blackwelder, 1991) is adopted for more accurate calculation. Furthermore, there might be some erroneous vectors depending on the size of correlation area and the

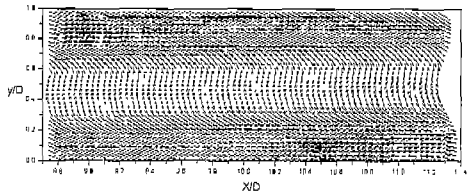

Fig. 4 Time-mean velocity distribution with swirl for Re=10,000 at X/D=10

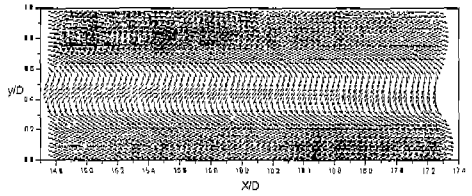

Fig. 5 Time-mean velocity distribution with swirl for Re=10,000 at X/D=16

distance of the searching area. Therefore, an error vector elimination method (Hojo and Takashima, 1995) based on the continuous flow condition was adopted.

4. Experimental Results and Discussion

4.1 Axial velocity distribution

This section is concerned with the presentation of axial velocity components and the fluctuating counterparts. All measurements presented were obtained using the PIV technique. From the velocity vector, the time average velocity components made dimensionless with respect to the average axial velocity will be appear first followed by the fluctuating components.

Figures 4~10 show the data of velocity vectors , which were measured for Re=10,000 at X/D=10, 16, 24, 30, 36, 44, and 50 by the PIV method. Even though the flow shows intensive swirling at the inlet of the test tube, its swirl flow intensity is gradually reduced according to the flow thruough tube, and at the end of tube the swirling movement is diminished and changed to a uniform flow.

Some of first measurements indicated that over the first 4 diameter, two regions of flow reversal were set up (the so called 2-cell structure). When

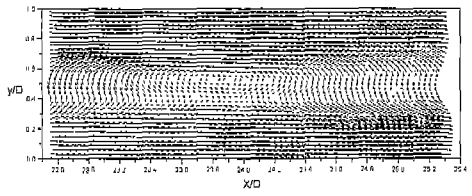

Fig. 6 Time-mean velocity distribution with swirl for Re=10,000 at X/D=24

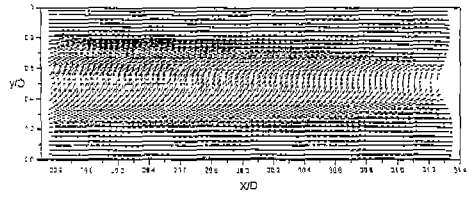

Fig. 7 Time-mean velocity distribution with swirl for Re=10,000 at X/D=30

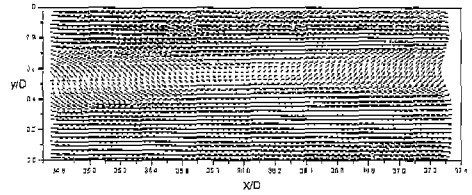

Fig. 8 Time-mean velocity distribution with swirl for Re=10,000 at X/D=36

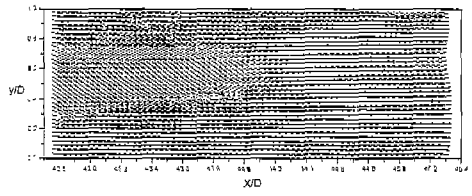

Fig. 9 Time-mean velocity distribution with swirl for Re=10,000 at X/D=44

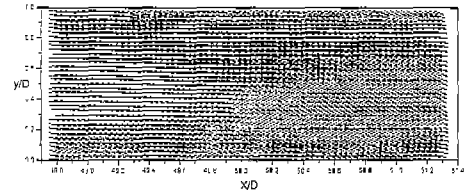

Fig. 10 Time-mean velocity distribution with swirl for Re=10,000 at X/D=50

the Reynolds number was higher, the intensity of swirling at the tube inlet was increased. By this effect, it can be considered that there is negative

velocity at the tube inlet. The sequence of velocity distributions show on Fig. 10 clearly demonstrates that flow reversal becomes diminished and finally disappears with axial distance from the inlet, as the swirl is reduced (i. e. as L/D increases). There shows some unrealistic velocity values near the wall. It is estimated that this was mainly due to several factors in which the resolution of the used camera was not so high enough to detect the flow motions of the wall boundary maintaining the size of the measurement area, and the window size to be correlated for PIV calculation was set relatively larger in order not to produce erroneous vectors.

Figures 11~13 show the axial velocity profiles, when the velocity vector is calculated as the local velocity at Re=10,000, 15,000 and 20,000. It shows a similar result with that of the axial velocity, reported so far. As it were, it shows the maximum velocity at the wall of the tube, and the negative velocity at the center of the tube. Furthermore, velocity is gradually reduced along the test tube, and at the end of the tube the swirling flow is diminished. This result shows normal turbulent flow with non-swirling flow. The main feature, that being of flow reversal over the central portion of the flow field, has already been referred to earlier. The sequence of velocity distributions shown on Figs. 11, 12 and 13 clearly demonstrates that flow reversal becomes diminished and finally disappears with axial distance from the inlet, as the inlet swirl is reduced. Although King et al. (1969) measured his axial velocity distribution using a pitot probe at a Reynolds number of 15, 000 the similarity in flow fields is quite clear.

The effect of increasing the Reynolds number is to move the position of maximum velocity towards the tube wall and produce more flow reversal at the center of the test tube. Figure 14 shows the dimensionless variations of the axial velocity components for the same range of Reynolds number as presented above. Wesk's , King's and Khodada's(1987) results have been included on the diagrams for a Reynolds number of 20, 000 and it can be seen again that the results of the first reference are in resonable agreement

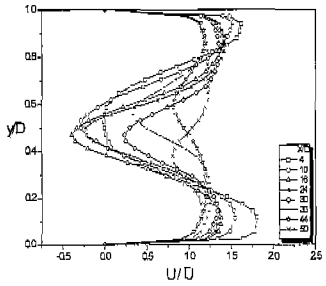

Fig. 11 Axial velocity profile for Re=10,000 with swirl across the test tube

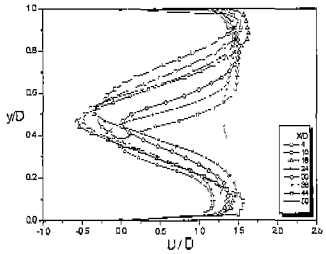

Fig. 12 Axial velocity profile for Re=15,000 with swirl across the test tube

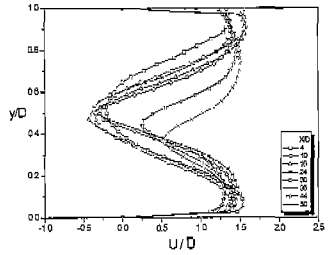

Fig. 13 Axial velocity profile for Re=20,000 with swirl across the test tube

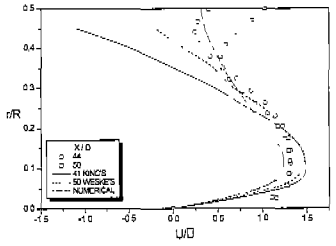

Fig. 14 Comparison of experimental and numerical axial velociy profiles with swirl for Re= 20,000

with the present work. However, some disagreement exists with the results of King's and Khodada's, particularly in the region where flow

reversal takes place. This is attributed to the inaccuracies inherent the pitot tube method of velocity measurement in such regions. The comparison to the numerical work of Khodada's (1987) will be brief due to the lack of detailed inlet conditions. In general, the agreement of the measurements to the computations is reasonable except for the reversal zone.

Generally, the shape of the presented velocity profiles are similar to those obtained by King et al. (1969), Weske et al. (1984) and Medwell (1989).

4.2 Turbulence intensity profiles

Figure 15 shows the time mean turbulence intensity without swirl for Re=10,000 at X/D=30. This figure illustrates the radial distributions of axial components of turbulence intensity. The axial turbulence intensity is shown as maximum at the tube wall, and minimum at the tube center. Also, a comparison of turbulence intensity is presented in Fig. 16 for Reynolds 10,000 and 20,000 without swirl. It shows a similar result with that of the axial turbulence intensity, reported so far.

Figure 17 indicates the time mean turbulence intensity with swirl for Re=10, 000 and axial turbulence intensity are shown in Figs. 18 , 19 and 20 for Re=10,000, 15,000 and 20,000 respectively. A particular feature of the turbulence intensities is the high values measured near the tube centre line where a highly turbulent core is present.

Nuttal(1953) was the first one to observe the reverse flow characteristics of a swirling flow in a circular tube. For Reynolds numbers in the range $1\times10^4\sim3\times10^4$, three types of flow patterns were observed as shown in Figs. 11~14 and 18~20. In the work, it was found that two cell vortex structure occurred at Re=15,000~Re=20,000.

In the most cases it appears that the turbulence intensities decrease with distance along the test tube, which is compatible with the decay of the swirl.

As would be expected, all of the distributions reflect the level of turbulence intensity, where large values are produced near the solid surface and even larger values near the center line of the

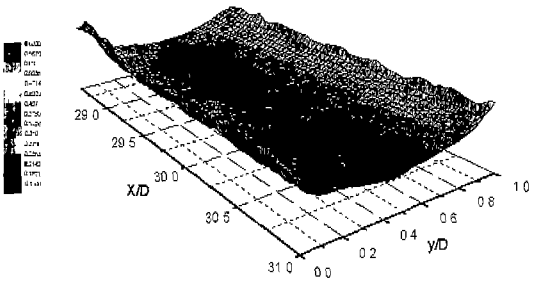

Fig. 15 Time-mean turbulence intensity without swirl for Re=10,000 at X/D=30

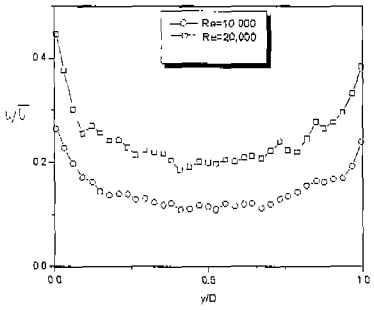

Fig. 16 Time-mean turbulence intensity without swirl at X/D=30

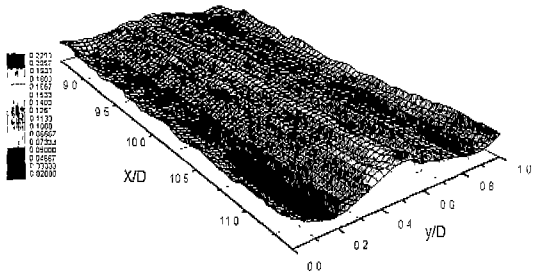

Fig. 17 Time-mean turbulence intensity swirl for Re=10,000 at X/D=10

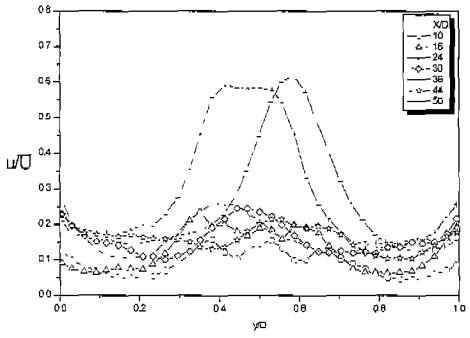

Fig. 18 Time-mean turburance intensity profile for Re=10,000 with swirling flow

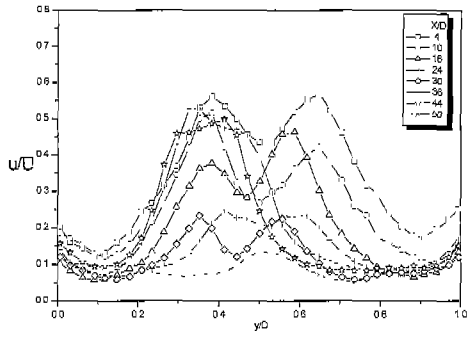

Fig. 19 Time-mean turbulence intensity profile for Re=15,000 with swirling flow

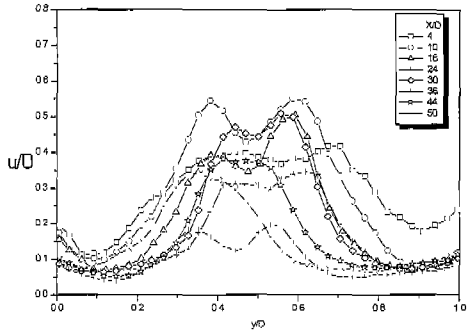

Fig. 20 Time-mean turbulence intensity profile for Re=20,000 with swirling flow

test tube. This position corresponds to that where flow reversal occurs in the axial direction.

5. Conclusion

From the above distributed experimental results the following was observed: It shows that the axial velocity profile of swirling flow, measured by the PIV method, is similar to that, reported so far. In general, the shape of the presented axial velocity profiles are similar to those obtained by King's , Weske's , Medwell's and Khodadai's.

In the most cases it appears that the turbulence intensities decrease with distance along the test tube, which is compatible with the decay of the swirl.

As would be expected, all of the distributions reflect the level of turbulence intensity, where large values are produced near the solid surface and even larger values near the centre line of the test tube. This position corresponds to that where flow reversal occurs in the axial direction.

References

Binnie, A. M. and Tear, J. D., 1955, "Experimental Measurement of Flow Swirling Water Through a Pressure Nozzle and Open Trumpet," *Proc. of the Royal society*, Vol, 235A, pp. 78~88.

Binnie, A. M., 1957, "Experimentals on the Slow Swirling Flow of a Viscous Liquid Through a Tube," *Quart. J. of Mech. and Applied Math.*, Vol, X, PT, 3.

Cigier, N. A. and Chervinsky, A., 1967, "Experimental Investigation of Swirling Vortex Motion in Jet," *J. of Mechanics ASME*, Vol, 34, pp. 443~451.

Hojo K. and Takashima H., 1995, "Detection of Erroneous Velocity Vectors Obtained in PIV," *J. of Visualization Society of Japan*, Vol, 15, Suppl. No. 2, 177.

Kimura I., Takamori T. and Inoue T., 1986, "Image Processing Instrumentation of Flow by Using Correlation Technique," *Flow Visualization*, Vol, 6, No. 22, 105.

King, M. K., Rothfus, R. R. and Kermode, R. I., 1969, "Static Pressure and Velocity Profiles in Swirling Incompressible Tube Flow," *J. of AICHE*, Vol, 15, No. 6, pp. 837~842.

Kobayashi, T., Saga, T., Haeno, T., Tsuda, N., 1991, "Development of a Real-Time Velocity Measurement System for High Reynolds Fluid Flow Using a Digital Image Processing Design, Experimental and Numerical Flow Visualization (Ed Khalighia B et al.)," ASME FED No. 128, pp. 9~14.

Khodadadai J. M. and Vlachos N. S., 1987, "Computation of Confined Swirling Flow: Effects of Boundary Conditions and Turbulence Model," *Numerical method in laminar and turbulent flow*, pp. 458~469.

Lilley, D. G., 1973, "Prediction of Inert Turbulent Swirl Flow," *AIAA*, Vol, 11, NO. 7, pp. 955~960.

Medwell J. O., Chang T. H. and Kown S. S., 1989, "A Study of Swirling Flow in a Cylindrical

Tube," *J. of SAREK*, Vol, 4, pp. 256~275.

Nuttall, J. B., 1953, "Axial Flow in a Vortex," *Natural*, Vol, 172, pp. 582~583.

Roberts, L. W., 1971, "The Prediction of Turbulent Swirling Pipe Flow," Report. EF/TN/A/37, Dept. of Mechanical Eng., Imperial College, London.

Rose, G. W., 1962, "A Swirling Round Turbulent Jet-Mean Flow Measurements," *J. of Appl. Mech*,. Vol, 29, pp. 615~625.

Sparrow, E. M. and Chaboki, A., 1984, "Swirl -Affected Fluid Flow and Heat Transfer in a Circular Tube," *J. OF Heat Transfer*, Vol, 106, pp. 766~773.

"Thinker's EYES," TNTech Co. Ltd., http://www.tientech.com/

Utami T., Blackwelder R., 1991, "A Cross Correlation Technique for Velocity Field Extraction from Particulate Visualization," *Exp. in Fluids*, Vol, 10, pp. 213~223.

Weske, D. R. and Sturov. G. Y. E., 1984, "Experimental Study of Flow Reattachment in a Single Sided Sudden Expansion," *NASA Cont. Rep*. MD - 41, Stanford University.

Wolf, L. Jr., Lavan, Z., and Fejer, A. A., 1969, "Measurement of the Decay of Swirl in Turbulent Flow," *J. of AIAA*, Vol, 7, No. 3, pp. 971~973.